

DiG: Scalable and Efficient Diffusion Models with Gated Linear Attention

Lianghui Zhu^{1,2,◇} Zilong Huang²✉ Bencheng Liao¹ Jun Hao Liew² Hanshu Yan²
Jiashi Feng² Xinggang Wang¹✉

¹ School of EIC, Huazhong University of Science & Technology ² ByteDance

Code & Models: [hustvl/DiG](https://github.com/hustvl/DiG)



Figure 1. Image generation with the proposed Diffusion Gated Linear Attention Transformers (DiG). We show selected samples from our class-conditional DiG-XL/2 models trained on ImageNet at 512×512 and 256×256 resolution, respectively.

Abstract

Diffusion models with large-scale pre-training have achieved significant success in the field of visual content generation, particularly exemplified by Diffusion Trans-

formers (DiT). However, DiT models have faced challenges with quadratic complexity efficiency, especially when handling long sequences. In this paper, we aim to incorporate the sub-quadratic modeling capability of Gated Linear Attention (GLA) into the 2D diffusion backbone. Specifically, we introduce Diffusion Gated Linear Attention Transformers (DiG), a simple, adoptable solution with minimal parameter overhead. We offer two variants, i.e., a plain and U-shape architecture, showing superior efficiency and

◇ This work was done when Lianghui Zhu was interning at ByteDance. ✉ Corresponding authors: Xinggang Wang (xgwang@hust.edu.cn) and Zilong Huang (zilong.huang2020@gmail.com)

competitive effectiveness. In addition to superior performance to DiT and other sub-quadratic-time diffusion models at 256×256 resolution, DiG demonstrates greater efficiency than these methods starting from a 512 resolution. Specifically, DiG-S/2 is $2.5\times$ faster and saves 75.7% GPU memory compared to DiT-S/2 at a 1792 resolution. Additionally, DiG-XL/2 is $4.2\times$ faster than the Mamba-based model at a 1024 resolution and $1.8\times$ faster than DiT with FlashAttention-2 at a 2048 resolution.

1. Introduction

In recent years, diffusion models [4, 20, 52, 55, 60] have emerged as potent deep generative models [13, 48] renowned for their ability to generate high-quality images. Their rapid evolution has spurred extensive applications across various fields, including image-to-image generation [8, 64], text-to-image generation [19, 46, 50], speech synthesis [7, 29], video generation [21, 33, 35], and 3D generation [42, 65]. Concurrent with the rapid development of sampling algorithms [32, 37, 53], the principal techniques have evolved into two main categories based on their architectural backbones: U-Net-based methods [20, 54] and ViT-based methods [14]. U-Net-based approaches continue to leverage the convolutional neural network (CNN) architecture [31, 49], whose hierarchical feature modeling ability benefits visual generation tasks. On the other hand, ViT-based methods [1, 38, 63] innovate by incorporating self-attention mechanisms [58] instead of traditional sampling blocks, resulting in streamlined yet effective performance.

Due to their excellent scalability in terms of performance, ViT-based methods [38] have been adopted as backbones in the most advanced diffusion works, including PixArt [5, 6], Sora [3], Stable Diffusion 3 [15], *etc.* However, the self-attention mechanism in ViT-based architectures scales quadratically with the input sequence length, making them resource-intensive when dealing with long sequence generation tasks, *e.g.*, high-resolution image generation and video generation. Recent works such as Mamba [18], RWKV [39] and Gated Linear Attention Transformer (GLA) [62], try to improve the long-sequence processing efficiency by integrating Recurrent Neural Network (RNN) like architecture and hardware-aware algorithms. Since a data-dependent gating mechanism is crucial for 1D modeling [44], GLA shows outstanding performance among the above methods.

Motivated by the success of GLA in the natural language processing domain, it is appealing that we can transfer this success from language generation to visual content generation by designing a scalable and efficient diffusion backbone with the advanced linear attention [10, 25, 26] method. However, visual generation with linear models, such as Mamba, RWKV, and GLA, often faces two challenges, *i.e.*,

unidirectional scanning modeling and lack of local awareness. Previous approaches [16, 23] have often addressed the first issue by performing bidirectional scanning within the same block. Nevertheless, such methods result in a significant increase in time consumption and numerical instability. To address these challenges, we propose Diffusion GLA (DiG), which incorporates a lightweight spatial reorient & enhancement module (SREM) for block-wise scanning direction controlling and local awareness. For the first issue, SREM changes the sequence direction with minimal number of matrix operations and assigns different scanning in a block-by-block manner. The scanning directions contain four basic patterns and enable each patch in sequences to be aware of other patches following 4 directions. For the second issue, we also incorporate a depth-wise convolution (DWConv) [9] in the SREM to provide local awareness with extremely small amounts of parameters. Inspired by U-Net [49], we further propose a U-shape variant of DiG and analyze the improvements. Crucially, this paper presents a systematic ablation study and a comprehensive evaluation of the proposed modules and architectures. It is important to highlight that DiG adheres to the first practices of linear attention transformers in diffusion generation, demonstrating superior efficiency in quadratic and sub-quadratic diffusion models.

Compared with the ViT-based method, *i.e.*, DiT [38], DiG presents competitive performance on ImageNet [12] 256×256 generation when using the same hyperparameters. Furthermore, DiG is more efficient in terms of training speed and GPU memory starting from a 512 resolution. The efficiency in terms of memory and speed empowers DiG to alleviate the resource constraint problem of long-sequence visual generation tasks. Specifically, DiG demonstrates significant efficiency improvements over comparable models: DiG-S/2 achieves a $2.5\times$ faster training speed and saves 75.7% GPU memory compared to DiT-S/2 at a 1792×1792 resolution as shown in Fig. 2. Furthermore, with the same model size, DiG-XL/2 is $4.2\times$ faster than the recent Mamba-based diffusion model at 1024 resolution and $1.8\times$ faster than DiT with well-designed CUDA-optimized FlashAttention-2 [11] at 2048 resolution as shown in Fig. 3.

Our main contributions can be summarized as follows:

- We propose Diffusion GLA (DiG), which incorporates an efficient DiG block for both global visual context modeling through block-wise scanning, and local visual awareness. To the best of our knowledge, DiG is the first exploration for diffusion backbone with linear attention.
- Without the burden of quadratic attention, the proposed DiG exhibits higher efficiency in both training speed and GPU memory cost while maintaining a similar modeling ability as DiT. Notably, DiG is $4.2\times$ faster than

Multi-path scanning and summation can easily lead to numerical NaN during training [16].

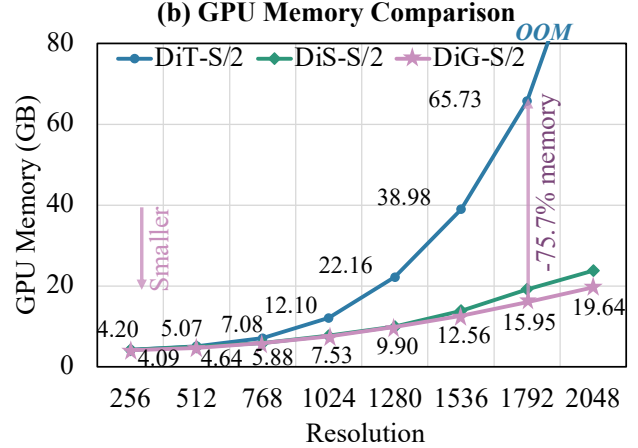
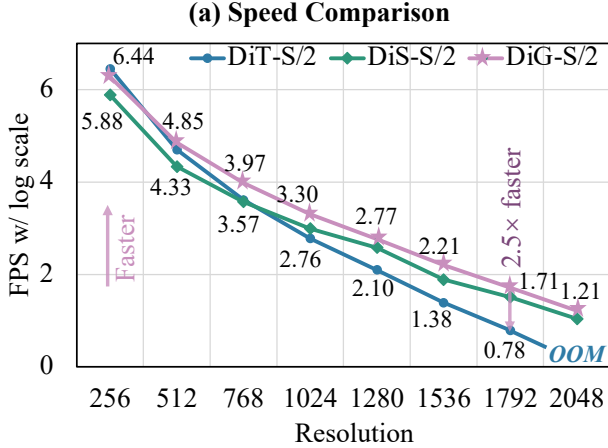


Figure 2. Efficiency comparison among DiT [38] with Attention [58], DiS [16] with Mamba [18], and our DiG model. DiG achieves higher training speed while costs lower GPU memory in dealing with high-resolution images. For example, DiG is 2.5× faster than DiT and saves 75.7% GPU memory with a resolution of 1792 × 1792, i.e., 12544 tokens per image. Patch size for all models is 2.

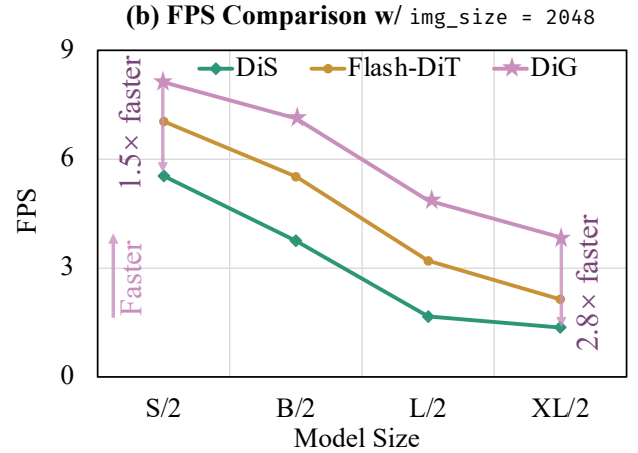
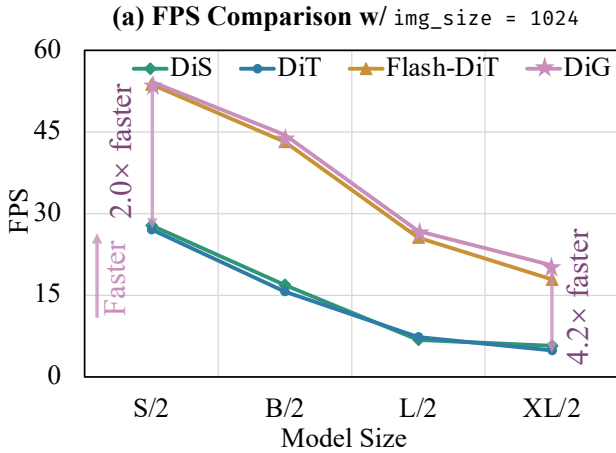


Figure 3. FPS comparison among DiS [16] with Mamba [18], DiT [38] with Attention [58], DiT with Flash Attention-2 (Flash-DiT) [11] and our DiG model varying from different model sizes. We take DiG as a baseline. With a resolution of 1024 × 1024, DiG is 2.0× faster than DiS at small size while 4.2× faster at XL size. Furthermore, DiG-XL/2 is 1.8× faster than the most well-designed high-optimized Flash-DiT-XL/2 with a resolution of 2048 × 2048.

the Mamba-based diffusion model at 1024 resolution and 1.8× faster than DiT with well-designed CUDA-optimized FlashAttention-2 [11] at 2048 resolution.

- We conduct extensive experiments on the ImageNet 256 × 256. The results demonstrate that DiG presents scalable ability and achieves comparable performance when compared with DiT. Besides, higher efficiency makes DiG promising to serve as the next-generation backbone for diffusion models in the context of large-scale long-sequence generation.

2. Related Work

2.1. Linear Attention Transformer

Different from standard autoregressive Transformer [59] which models the global attention matrix, the original lin-

ear attention [26] is essentially a linear RNN with matrix-valued-format hidden states. Linear attention introduces a similarity kernel $k(x, y)$ with an associated feature map $\phi(\cdot)$, i.e., $k(x, y) = \langle \phi(x), \phi(y) \rangle$. The calculation of output $\mathbf{O} \in \mathbb{R}^{L \times d}$ (here L is the sequence length and d is the dimension) can be represented as follows:

$$\mathbf{O}_t = \frac{\sum_{i=1}^t k(\mathbf{Q}_t, \mathbf{K}_i) \mathbf{V}_i}{\sum_{i=1}^t k(\mathbf{Q}_t, \mathbf{K}_i)} = \frac{\phi(\mathbf{Q}_t) \sum_{i=1}^t \phi(\mathbf{K}_i)^\top \mathbf{V}_i}{\phi(\mathbf{Q}_t) \sum_{i=1}^t \phi(\mathbf{K}_i)^\top}, \quad (1)$$

$$\mathbf{S}_t = \mathbf{S}_{t-1} + \phi(\mathbf{K}_i) \mathbf{V}_i, z_t = z_{t-1} + \phi(\mathbf{K}_i)^\top, \mathbf{O}_t = \frac{\phi(\mathbf{Q}_t) \mathbf{S}_t}{\phi(\mathbf{Q}_t) z_t}, \quad (2)$$

where query \mathbf{Q} , key \mathbf{K} , value \mathbf{V} have shapes of $L \times d$ and t is the index of current token. By denoting hidden state $\mathbf{S}_t = \sum_{i=1}^t \phi(\mathbf{K}_i) \mathbf{V}_i$ and normalizer $z_t = \sum_{i=1}^t \phi(\mathbf{K}_i)^\top$ where

$\mathbf{S}_t \in \mathbb{R}^{d \times d}$, $z_t \in \mathbb{R}^{d \times 1}$, the Eq. (1) can be rewritten as the Eq. 2. Recent works set $\phi(\cdot)$ to be the identity [34, 56] and remove z_t [43], resulting linear attention Transformer with the following format:

$$\mathbf{S}_t = \mathbf{S}_{t-1} + \mathbf{K}_t^\top \mathbf{V}_t, \quad \mathbf{O}_t = \mathbf{Q}_t \mathbf{S}_t. \quad (3)$$

Directly using a linear attention Transformer for visual generation leads to poor performance due to the unidirectional modeling, so we propose a lightweight spatial reorient & enhancement module to take care of both modeling global context in four directions block by block and local information.

2.2. Backbones in Diffusion Models

Existing diffusion models typically employ U-Net as backbones [17, 20, 47] for image generation. Recently, Vision Transformer (ViT)-based backbones [1, 3, 5, 6, 38] receive significant attention due to the scalability of transformer and its natural fit for multi-modal learning. However, ViT-based architectures suffer from quadratic complexity, limiting their practicability in long sequence generation tasks, such as high-resolution image synthesis, video generation *etc.* To mitigate this, recent works explore subquadratic-time approaches to efficiently handle long sequences. For example, DiS [16], DiffuSSM [61], and ZigMa [23] employ state-space models as diffusion backbones for better computation efficiency. Diffusion-RWKV [61] adopt an RWKV architecture in diffusion models for image generation.

Our DiG also follows this line of research, aiming at improving the efficiency of long sequence processing by adopting Gated Linear Attention Transformer (GLA) as diffusion backbones. Our proposed adaptation maintains the fundamental structure and benefits of GLA while introducing a few crucial modifications necessary for generating high-fidelity visual data.

3. Method

3.1. Preliminaries

Gated Linear Attention Transformer. The Gated Linear Attention Transformer (GLA) [62] combines a data-dependent gating mechanism and linear attention, achieving superior recurrent modeling performance. Given an input $\mathbf{X} \in \mathbb{R}^{L \times d}$ (here L is the sequence length and d is the dimension), GLA calculates the query, key, and value vectors as follows:

$$\mathbf{Q} = \mathbf{XW}_Q, \mathbf{K} = \mathbf{XW}_K, \mathbf{V} = \mathbf{XW}_V, \quad (4)$$

where \mathbf{W}_Q , \mathbf{W}_K , and \mathbf{W}_V are linear projection weights. The dimension number of \mathbf{Q} , \mathbf{K} is d_k , and d_v is for \mathbf{V} . Next, GLA compute the gating matrix \mathbf{G} as follows:

$$\mathbf{G}_t = \alpha_t^\top \beta_t \in \mathbb{R}^{d_k \times d_v}, \alpha = \sigma(\mathbf{XW}_\alpha + b_\alpha)^{\frac{1}{\tau}} \in \mathbb{R}^{L \times d_k}, \quad (5)$$

$$\beta = \sigma(\mathbf{XW}_\beta + b_\beta)^{\frac{1}{\tau}} \in \mathbb{R}^{L \times d_v}, \quad (6)$$

where t is the index of token, σ is the sigmoid function, b is the bias term, and $\tau \in \mathbb{R}$ is a temperature term. As shown in Fig. 4, the final output \mathbf{Y}_t is obtained as follows:

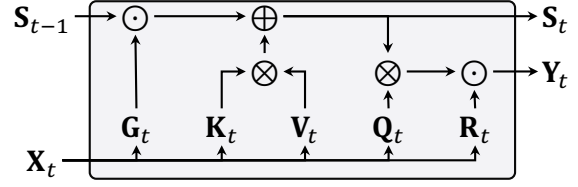


Figure 4. Pipeline of GLA.

$$\mathbf{S}'_{t-1} = \mathbf{G}_t \odot \mathbf{S}_{t-1} \in \mathbb{R}^{d_k \times d_v}, \quad (7)$$

$$\mathbf{S}_t = \mathbf{S}'_{t-1} + \mathbf{K}_t^\top \mathbf{V}_t \in \mathbb{R}^{d_k \times d_v}, \quad (8)$$

$$\mathbf{O}_t = \mathbf{Q}_t^\top \mathbf{S}_t \in \mathbb{R}^{1 \times d_v}, \quad (9)$$

$$\mathbf{R}_t = \text{Swish}(\mathbf{X}_t \mathbf{W}_r + b_r) \in \mathbb{R}^{1 \times d_v}, \quad (10)$$

$$\mathbf{Y}_t = (\mathbf{R}_t \odot \text{LN}(\mathbf{O}_t)) \mathbf{W}_O \in \mathbb{R}^{1 \times d}, \quad (11)$$

where Swish is the Swish [45] activation function, and \odot is the element-wise multiplication operation. In subsequent sections, we use $\mathbf{GLA}(\cdot)$ to refer to the gated linear attention computation for the input sequence.

Diffusion Models. Before introducing the proposed method, we provide a brief review of diffusion models (DDPM) [20]. The DDPM takes noise as an input and samples images by iterative denoising the input. The forward process of DDPM begins with a stochastic process where the initial image x_0 is gradually corrupted by noise and is finally transformed into a simpler, noise-dominated state. The forward noising process can be represented as follows:

$$q(x_{1:T} | x_0) = \prod_{t=1}^T q(x_t | x_{t-1}), \quad (12)$$

$$q(x_t | x_0) = \mathcal{N}(x_t; \sqrt{\alpha_t} x_0, (1 - \alpha_t) I), \quad (13)$$

where $x_{1:T}$ is the sequence of noised images from time $t = 1$ to $t = T$. Then, DDPM learns the reverse process that recovers the original image with learned μ_θ and Σ_θ :

$$p_\theta(x_{t-1} | x_t) = \mathcal{N}(x_{t-1}; \mu_\theta(x_t), \Sigma_\theta(x_t)), \quad (14)$$

where θ are the parameters of the denoiser, and are trained with the variational lower bound [52] on the loglikelihood of the observed data x_0 .

$$\begin{aligned} \mathcal{L}(\theta) = & -p(x_0 | x_1) \\ & + \sum_t D_{KL}(q^*(x_{t-1} | x_t, x_0) \| p_\theta(x_{t-1} | x_t)), \end{aligned} \quad (15)$$

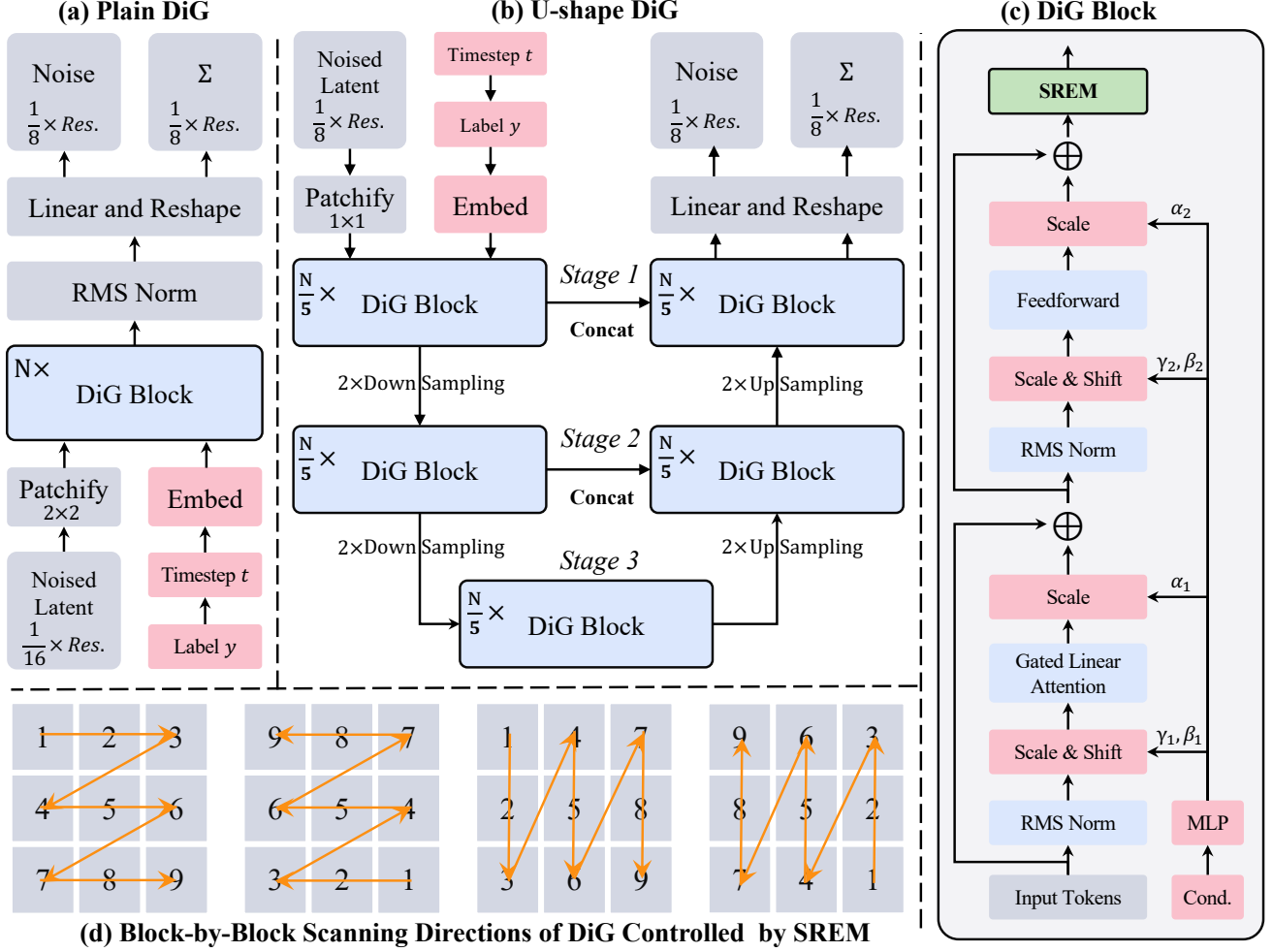


Figure 5. The overview of the proposed DiG models. The figure presents the (a) plain DiG, denoted as DiG, (b) U-shape DiG, denoted as U-DiG, (c) DiG block, and (d) block-by-block scanning directions of DiG controlled by the SREM.

where \mathcal{L} is the full loss. To further simplify the training process of DDPM, researchers reparameterize μ_θ as a noise prediction network ϵ_θ and minimize the mean squared error loss $\mathcal{L}_{\text{simple}}$ between $\epsilon_\theta(x_t)$ and the true Gaussian noise ϵ_t :

$$\mathcal{L}_{\text{simple}}(\theta) = \|\epsilon_\theta(x_t) - \epsilon_t\|_2^2. \quad (16)$$

However, to train a diffusion model that can learn a variable reverse process covariance Σ_θ , we need to optimize the full D_{KL} term. In this paper, we follow DiT [38]’s training recipe where we use the simple loss $\mathcal{L}_{\text{simple}}$ to train the noise prediction network ϵ_θ and use the full loss \mathcal{L} to train the covariance prediction network Σ_θ . After the training process, we follow the stochastic sampling process to generate images from the learned ϵ_θ and Σ_θ .

3.2. Diffusion GLA

We present two variants of Diffusion GLA (DiG), as shown in Fig. 5. Our goal is to be as faithful to the standard GLA architecture as possible to retain its scaling ability and high-efficiency properties. We follow some of the best practices

of previous vision transformer architectures [1, 14, 38] to propose plain DiG and U-shape DiG, which are denoted as DiG and U-DiG, respectively. DiG first takes a spatial representation z output by the VAE encoder [28, 47] as input. For example, given a $256 \times 256 \times 3$ image, we obtain a spatial representation z of shape $32 \times 32 \times 4$ after the VAE encoder. DiG subsequently converts this spatial input into a token sequence $\mathbf{z}_p \in \mathbb{R}^{T \times (P^2 \cdot C)}$ through a patchify layer, where T is length of token sequence, C is the number of spatial representation channels, P is the size of image patches, and halving P will quadruple T . Specifically, p for DiG is 2, while for U-DiG, p is 1. Next, we linearly project the \mathbf{z}_p to the vector with dimension D and add frequency-based positional embeddings $\mathbf{E}_{pos} \in \mathbb{R}^{T \times D}$ to all projected tokens as follows:

$$\mathbf{z}_0 = [\mathbf{z}_p^1 \mathbf{W}; \mathbf{z}_p^2 \mathbf{W}; \dots; \mathbf{z}_p^T \mathbf{W}] + \mathbf{E}_{pos}, \quad (17)$$

where \mathbf{z}_p^t is the t -th patch of \mathbf{z}_p , $\mathbf{W} \in \mathbb{R}^{(P^2 \cdot C) \times D}$ is the learnable projection matrix. As for conditional information

such as noise timesteps $t \in \mathbb{R}$, and class labels $y \in \mathbb{R}$, we adopt multi-layer perception (MLP) and embedding layer as timestep embedder and label embedder, respectively.

$$\mathbf{t} = \text{MLP}(t), \quad \mathbf{y} = \text{Embed}(y), \quad (18)$$

where $\mathbf{t} \in \mathbb{R}^{1 \times D}$ is time embedding and $\mathbf{y} \in \mathbb{R}^{1 \times D}$ is label embedding. We then send the token sequence (\mathbf{z}_{l-1}) to the l -th block of the DiG encoder, and obtain the output \mathbf{z}_l . For the U-DiG variant, there are down-sampling and up-sampling modules between different stages, and shortcuts in the same stage. Finally, we normalize the output token sequence \mathbf{z}_L , and feed it to the linear projection head to get the final predicted noise $\hat{\mathbf{p}}_{noise}$ and predicted covariance $\hat{\mathbf{p}}_{covariance}$, as follows:

$$\mathbf{z}_l = \text{DiG}_l(\mathbf{z}_{l-1}, \mathbf{t}, \mathbf{y}), \quad \mathbf{z}_n = \text{Norm}(\mathbf{z}_L), \quad (19)$$

$$\hat{\mathbf{p}}_{noise}, \hat{\mathbf{p}}_{covariance} = \text{Linear}(\mathbf{z}_n), \quad (20)$$

where DiG_l is the l -th diffusion GLA block, L is the number of blocks, and Norm is the normalization layer. The $\hat{\mathbf{p}}_{noise}$ and $\hat{\mathbf{p}}_{covariance}$ have the same shape as the input spatial representation, *i.e.*, $32 \times 32 \times 4$.

3.3. DiG Block

The original GLA block processes input sequence in a recurrent manner, which only enables causal modeling for 1-D sequence. Previous methods [16, 23] employ multi-path scanning within the same block to model global context, but this leads to a significant increase in time consumption and numerical instability [16], as shown in Table 1. To model the global context efficiently, we introduce the DiG block as shown in Fig. 5, which incorporates a spatial reorient & enhancement module (SREM) that enables lightweight spatial recognition and controls block-wise scanning directions.

Specifically, we present the forward process of DiG block in Algo. 1. Following the widespread usage of adaptive normalization layers [40] in GANs [2, 24] and diffusion models [13, 38], we add and normalize the input timestep embedding \mathbf{t} and label embedding \mathbf{y} to regress the scale parameter α , γ , and shift parameter β . Next, we launch gated linear attention (GLA) and feedforward network (FFN) with the adjustment of regressed adaptive layer norm (adaLN) parameters. Then, we reshape the sequence to 2D and launch a lightweight 3×3 depth-wise convolution (DWConv2d) layer to perceive local spatial information. However, we notice that using traditional initialization for DWConv2d leads to slow convergence because convolutional weights are dispersed around. To address this problem, we use identity initialization that only sets the convolutional kernel center as 1, and the surroundings to 0. Lastly, we alternate transpose and flip operations block-by-block to efficiently control block-wise scanning directions using minimal number of matrix operations.

	Extra Operations		If Stable?	Time (s)
	Matrix OPs	Scanning		
Bidirectional	3	1	✗	2.18
4-directional	13	3	✗	4.02
Block-by-Block	2	0	✓	1.56

Table 1. Experimental results of different scanning strategies. Given $I = 32, p = 2$, all experiments are conducted with XL size models. Extra operations include matrix operations and scanning operations, which both increase the time consumption.

3.4. Architecture Details

We use N DiG blocks, each operating at the hidden dimension size D . Following previous works [14, 38, 62], we follow standard transformer setting that scales N , D , and attention heads number. Particularly, we provide four configurations: S, B, L, and XL, for the two different variants, as shown in the Table 2. They cover a wide range of flop allocations, ranging from 4.10 Gflops to 89.40 Gflops, presenting a way to gauge the scaling performance and efficiency. Notably, DiG consumes 70.8% to 76.3% Gflops, and U-DiG only consumes 66.0% to 67.6% Gflops when compared with the same model size DiT baselines. Both the proposed two variants are computationally efficient.

3.5. Efficiency Analysis

GPU contains two important components, *i.e.*, high bandwidth memory (HBM) and SRAM. HBM has a bigger memory size but SRAM has a larger bandwidth. To make full use of SRAM and modeling sequences in a parallel form, we follow GLA to split a whole sequence into many chunks that can complete calculations on SRAM. We denote the chunk size as M , the training complexity is thus $O(\frac{T}{M}(M^2D + MD^2)) = O(TMD + TD^2)$, which is less than the traditional attention’s complexity $O(T^2D)$ when $T > D$. Furthermore, the scaling analysis of speed and GPU memory are shown in Fig. 2 and Fig. 3, which demonstrate the high efficiency of the proposed DiG: DiG shows notable efficiency gains: DiG-S/2 is $2.5\times$ faster and saves 75.7% GPU memory compared to DiT-S/2 at 1792×1792 . Additionally, DiG-XL/2 is $4.2\times$ faster than the Mamba-based model at 1024 resolution and $1.8\times$ faster than DiT with FlashAttention-2 at 2048.

4. Experiment

4.1. Experimental Settings

Datasets and metrics. Following previous works [38], we use ImageNet [12] for class-conditional image generation learning at a resolution of 256×256 . The ImageNet dataset contains 1,281,167 training images varying from 1,000 different classes. We use horizontal flipping for data augmentation. We measure the generation performance with Frechet Inception Distance (FID) [36], Incep-

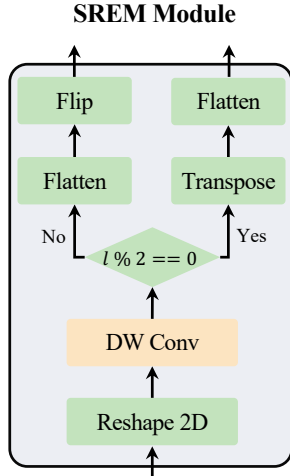


Figure 6. Details of the Spatial Reorient & Enhancement Module (SREM).

Algorithm 1: DiG Block Process.

Input: token sequence $\mathbf{z}_{l-1} : (\mathbf{B}, \mathbf{T}, \mathbf{D})$, timestep embed $\mathbf{t} : (\mathbf{B}, \mathbf{1}, \mathbf{D})$, label embed $\mathbf{y} : (\mathbf{B}, \mathbf{1}, \mathbf{D})$
Output: token sequence $\mathbf{z}_l : (\mathbf{B}, \mathbf{T}, \mathbf{D})$

- 1 $\alpha_1, \beta_1, \gamma_1, \alpha_2, \beta_2, \gamma_2 : (\mathbf{B}, \mathbf{1}, \mathbf{D}) \leftarrow \text{MLP}(\mathbf{t} + \mathbf{y})$ // regress parameters of adaLN
- 2 $\mathbf{z}'_{l-1} : (\mathbf{B}, \mathbf{T}, \mathbf{D}) \leftarrow \mathbf{z}_{l-1} + \alpha_1 \odot \text{GLA}(\text{Norm}(\mathbf{z}_{l-1}) \odot (1 + \gamma_1) + \beta_1)$
- 3 $\mathbf{z}''_{l-1} : (\mathbf{B}, \mathbf{T}, \mathbf{D}) \leftarrow \mathbf{z}'_{l-1} + \alpha_2 \odot \text{FFN}(\text{Norm}(\mathbf{z}'_{l-1}) \odot (1 + \gamma_2) + \beta_2)$
- 4 $\mathbf{z}'''_{l-1} : (\mathbf{B}, \sqrt{\mathbf{T}}, \sqrt{\mathbf{T}}, \mathbf{D}) \leftarrow \text{DWConv2d}(\text{reshape2d}(\mathbf{z}''_{l-1}))$ // SREM module
- 5 **if** $l \% 2 == 0$ **then**
- 6 $\mathbf{z}''''_{l-1} : (\mathbf{B}, \sqrt{\mathbf{T}}, \sqrt{\mathbf{T}}, \mathbf{D}) \leftarrow \text{transpose}(\mathbf{z}'''_{l-1})$ // transpose the token matrix every two block
- 7 $\mathbf{z}_l : (\mathbf{B}, \mathbf{T}, \mathbf{D}) \leftarrow \text{flatten}(\mathbf{z}''''_{l-1})$ // flatten the token matrix into 1-D sequence
- 8 **end**
- 9 **else**
- 10 $\mathbf{z}''_{l-1} : (\mathbf{B}, \mathbf{T}, \mathbf{D}) \leftarrow \text{flatten}(\mathbf{z}'''_{l-1})$ // flatten the token matrix into 1-D sequence
- 11 $\mathbf{z}_l : (\mathbf{B}, \mathbf{T}, \mathbf{D}) \leftarrow \text{flip}(\mathbf{z}''_{l-1})$ // flip the token sequence every two block
- 12 **end**
- 13 **Return:** \mathbf{z}_l

Model	Layers N	Hidden Size D	Gflops	$\frac{\text{Gflops}_{\text{DiG}}}{\text{Gflops}_{\text{DiT}}}$
DiG-S	12	384	4.30	70.8%
DiG-B	12	768	17.07	74.1%
DiG-L	24	1024	61.66	76.3%
DiG-XL	28	1152	89.40	75.3%
U-DiG-S	20	128	4.10	67.6%
U-DiG-B	20	256	15.20	66.0%
U-DiG-L	40	320	53.57	66.3%
U-DiG-XL	40	416	79.09	66.6%

Table 2. Details of DiG models. We follow DiT [38] model configurations for the Small (S), Base (B), Large (L), and XLarge (XL) variants. Given $l = 32, p = 2$ for DiG, $p = 1$ for U-DiG.

tion Score [51], sFID [36], and Precision/Recall [30].

Implementation details. We use AdamW optimizer with a constant learning rate of $1e - 4$. Following the previous works [38], we utilize the exponential moving average (EMA) of DiG weights during training with a decay rate of 0.9999. We generate all images with the EMA model. For the training of ImageNet, we use an off-the-shelf pretrained variational autoencoder (VAE) [27, 48].

4.2. Model Analysis

Effect of spatial reorient & enhancement module. As shown in Table 3, we analyze the effectiveness of the proposed spatial reorient & enhancement module (SREM). We take the DiT-S/2 as our baseline method. The naive plain DiG with only causal modeling has significantly fewer flops and parameters, but also poor FID performance due to the lack of global context. We first add the bidirectional scanning to DiG and observe significant improvement, *i.e.*, 69.28 FID, which demonstrates the importance of global context. Experiment without identity initialization

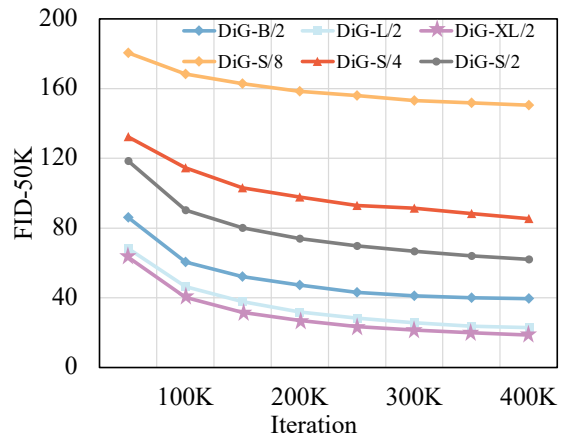


Figure 7. Scaling analysis with DiG model scales and patch sizes. For DWConv2d (the \blackstar symbol), leads to worse FID, while the DWConv2d with identity initialization can improve performance a lot. The experiment with DWConv2d proves the importance of identity initialization and local awareness. The experiment with full SREM brings the best performance, taking care of both local information and global context. Experiments in the last three rows indicate that the more suitable position for SREM is after the FFN.

Scaling model scales and patch sizes. We investigate the scaling ability of DiG among four different model scales and three patch sizes on the ImageNet dataset. As depicted in Fig. 7, the performance improves as the models scale from S/2 to XL/2 and the patch size from 2 to 8. The results demonstrate the scaling ability of DiG, indicating its potential as a large foundational diffusion model.

Structural ablation from DiG to U-DiG. We evaluate the structural benefits from DiG to U-DiG. As shown in

Model	Spatial Reorient & Enhancement Module			SREM Position	Flops (G)	Params (M)	FID-50K
	Bidirectional	DWConv2d	4-directional				
<i>Baseline Method.</i>							
DiT-S/2					6.06	33.0	68.4
<i>Ours.</i>							
DiG-S/2					4.29	33.0	175.84
DiG-S/2	✓			After FFN	4.29	33.0	69.28
DiG-S/2	✓	✗		After FFN	4.30	33.1	96.83
DiG-S/2	✓	✓		After FFN	4.30	33.1	63.84
DiG-S/2	✓	✓	✓	After FFN	4.30	33.1	62.06
DiG-S/2	✓	✓	✓	Before Attn.	4.30	33.1	62.34
DiG-S/2	✓	✓	✓	Between Attn. & FFN	4.30	33.1	62.93

Table 3. Ablation of the proposed Spatial Reorient & Enhancement Module (SREM). We validate the effectiveness of each SREM component and use the same hyperparameters for all models. The “half right and half wrong symbol” (✓) means use DWConv2d without the identity initialization. We mark the best result in **bold**.

Model	FID↓	sFID↓	IS↑	P↑	R↑
ADM [13]	10.94	6.02	100.98	0.69	0.63
ADM-U	7.49	5.13	127.49	0.72	0.63
ADM-G	4.59	5.25	186.70	0.82	0.52
ADM-G, ADM-U	3.94	6.14	215.84	0.83	0.53
CDM [22]	4.88	-	158.71	-	-
LDM-8 [48]	15.51	-	79.03	0.65	0.63
LDM-8-G	7.76	-	209.52	0.84	0.35
LDM-4-G	3.95	-	178.22	0.81	0.55
LDM-4-G	3.60	-	247.67	0.87	0.48
<i>Other sub-quadratic-time diffusion methods.</i>					
DiM-H/2 [57]	2.40	-	-	-	-
DiS-H/2 [16]	2.10	4.55	271.32	0.82	0.58
DiMSUM-L/2-G [41]	2.11	0.59	-	-	-
<i>Baselines and Ours.</i>					
DiT-S/2 (400K) [38]	68.40	-	-	-	-
DiG-S/2 (400K)	62.06	11.77	22.81	0.39	0.56
DiT-B/2 (400K)	43.47	-	-	-	-
DiG-B/2 (400K)	39.50	8.50	37.21	0.51	0.63
DiT-L/2 (400K)	23.33	-	-	-	-
DiG-L/2 (400K)	22.90	6.91	59.87	0.60	0.64
DiT-XL/2 (400K)	19.47	-	-	-	-
DiG-XL/2 (400K)	18.53	6.06	68.53	0.63	0.64
DiT-XL/2 (7M)	9.62	6.85	121.50	0.67	0.67
DiG-XL/2 (1.2M)	8.60	6.46	130.03	0.68	0.68
DiT-XL/2-G (7M)	2.27	4.60	278.24	0.83	0.57
DiG-XL/2-G (1.2M)	2.07	4.53	278.95	0.82	0.60

Table 4. Benchmarking class-conditional image generation on ImageNet 256×256 . DiG models adopt the same hyperparameters as DiT [38] for fair comparison. G is the classifier-free guidance. We mark the best results in **bold**.

Table 5, both the shortcut and hierarchical structures contribute positively to the metrics. Notably, for the generation task at a 512 resolution, U-DiG-S/1 achieves a remarkable improvement over DiG-S/2, with an FID gain exceeding 16.2, which demonstrates the effectiveness of U-DiG in generating high-resolution images.

	w/ short cut	w/ hierarchy	FID-50K	
			IN-256	IN-512
DiT-S/2			68.40	NaN
DiG-S/2			62.06	99.04
DiG-S/2	✓		57.01	91.42
U-DiG-S/1	✓	✓	52.20	82.62

Table 5. Structural ablation from DiG to U-DiG.

4.3. Main Results

We mainly compare the proposed plain DiG with DiT [38]. For class-conditional image generation on ImageNet 256×256 , as shown in Table 4, the proposed DiG has fewer FLOPs but outperforms DiT among four model scales with 400K training iterations with the same hyperparameters. Furthermore, the DiG-XL/2 (1.2M) with classifier-free guidance also presents competitive results when compared with concurrent sub-quadratic-time diffusion methods.

5. Conclusion

In this work, we present DiG, a cost-effective alternative to the vanilla Transformer for diffusion models in image generation tasks. In particular, DiG explores Gated Linear Attention Transformers (GLA), attaining comparable effectiveness and superior efficiency in long-sequence image generation tasks. Experimentally, DiG shows comparable performance to prior diffusion models on class-conditional ImageNet 256×256 benchmark while significantly reducing the computational burden starting from a 512 resolution. We hope this work can open up the possibility for other long-sequence generation tasks, such as video and audio modeling.

Limitations. Although DiG shows superior efficiency in diffusion image generation, building a large foundation model like Sora [3] upon DiG is still an area that needs to be explored further.

References

- [1] Fan Bao, Shen Nie, Kaiwen Xue, Yue Cao, Chongxuan Li, Hang Su, and Jun Zhu. All are worth words: A vit backbone for diffusion models. In *Proceedings of the IEEE/CVF Conference on Computer Vision and Pattern Recognition*, pages 22669–22679, 2023. 2, 4, 5
- [2] Andrew Brock, Jeff Donahue, and Karen Simonyan. Large scale gan training for high fidelity natural image synthesis. *arXiv preprint arXiv:1809.11096*, 2018. 6
- [3] Tim Brooks, Bill Peebles, Connor Holmes, Will DePue, Yufei Guo, Li Jing, David Schnurr, Joe Taylor, Troy Luhman, Eric Luhman, Clarence Ng, Ricky Wang, and Aditya Ramesh. Video generation models as world simulators. 2024. 2, 4, 8
- [4] Hanqun Cao, Cheng Tan, Zhangyang Gao, Yilun Xu, Guangyong Chen, Pheng-Ann Heng, and Stan Z Li. A survey on generative diffusion models. *IEEE Transactions on Knowledge and Data Engineering*, 2024. 2
- [5] Junsong Chen, Jincheng Yu, Chongjian Ge, Lewei Yao, Enze Xie, Yue Wu, Zhongdao Wang, James Kwok, Ping Luo, Huchuan Lu, et al. Pixart-alpha: Fast training of diffusion transformer for photorealistic text-to-image synthesis. *arXiv preprint arXiv:2310.00426*, 2023. 2, 4
- [6] Junsong Chen, Chongjian Ge, Enze Xie, Yue Wu, Lewei Yao, Xiaozhe Ren, Zhongdao Wang, Ping Luo, Huchuan Lu, and Zhenguo Li. Pixart-sigma: Weak-to-strong training of diffusion transformer for 4k text-to-image generation. *arXiv preprint arXiv:2403.04692*, 2024. 2, 4
- [7] Nanxin Chen, Yu Zhang, Heiga Zen, Ron J Weiss, Mohammad Norouzi, and William Chan. Wavegrad: Estimating gradients for waveform generation. *arXiv preprint arXiv:2009.00713*, 2020. 2
- [8] Jooyoung Choi, Sungwon Kim, Yonghyun Jeong, Youngjune Gwon, and Sungroh Yoon. Ilvr: Conditioning method for denoising diffusion probabilistic models. *arXiv preprint arXiv:2108.02938*, 2021. 2
- [9] François Chollet. Xception: Deep learning with depthwise separable convolutions. In *Proceedings of the IEEE conference on computer vision and pattern recognition*, pages 1251–1258, 2017. 2
- [10] Krzysztof Choromanski, Valerii Likhoshesterov, David Dohan, Xingyou Song, Andreea Gane, Tamas Sarlos, Peter Hawkins, Jared Davis, Afroz Mohiuddin, Lukasz Kaiser, et al. Rethinking attention with performers. *arXiv preprint arXiv:2009.14794*, 2020. 2
- [11] Tri Dao. Flashattention-2: Faster attention with better parallelism and work partitioning. *arXiv preprint arXiv:2307.08691*, 2023. 2, 3
- [12] Jia Deng, Wei Dong, Richard Socher, Li-Jia Li, Kai Li, and Li Fei-Fei. Imagenet: A large-scale hierarchical image database. In *2009 IEEE conference on computer vision and pattern recognition*, pages 248–255. Ieee, 2009. 2, 6
- [13] Prafulla Dhariwal and Alexander Nichol. Diffusion models beat gans on image synthesis. *Advances in neural information processing systems*, 34:8780–8794, 2021. 2, 6, 8
- [14] Alexey Dosovitskiy, Lucas Beyer, Alexander Kolesnikov, Dirk Weissenborn, Xiaohua Zhai, Thomas Unterthiner, Mostafa Dehghani, Matthias Minderer, Georg Heigold, Sylvain Gelly, et al. An image is worth 16x16 words: Transformers for image recognition at scale. *arXiv preprint arXiv:2010.11929*, 2020. 2, 5, 6
- [15] Patrick Esser, Sumith Kulal, Andreas Blattmann, Rahim Entezari, Jonas Müller, Harry Saini, Yam Levi, Dominik Lorenz, Axel Sauer, Frederic Boesel, et al. Scaling rectified flow transformers for high-resolution image synthesis. *arXiv preprint arXiv:2403.03206*, 2024. 2
- [16] Zhengcong Fei, Mingyuan Fan, Changqian Yu, and Junshi Huang. Scalable diffusion models with state space backbone. *arXiv preprint arXiv:2402.05608*, 2024. 2, 3, 4, 6, 8
- [17] Yunxiang Fu, Chaoqi Chen, and Yizhou Yu. Lamamba-diff: Linear-time high-fidelity diffusion models based on local attention and mamba. *arXiv preprint arXiv:2408.02615*, 2024. 4
- [18] Albert Gu and Tri Dao. Mamba: Linear-time sequence modeling with selective state spaces. *arXiv preprint arXiv:2312.00752*, 2023. 2, 3
- [19] Shuyang Gu, Dong Chen, Jianmin Bao, Fang Wen, Bo Zhang, Dongdong Chen, Lu Yuan, and Baining Guo. Vector quantized diffusion model for text-to-image synthesis. In *Proceedings of the IEEE/CVF Conference on Computer Vision and Pattern Recognition*, pages 10696–10706, 2022. 2
- [20] Jonathan Ho, Ajay Jain, and Pieter Abbeel. Denoising diffusion probabilistic models. *Advances in neural information processing systems*, 33:6840–6851, 2020. 2, 4
- [21] Jonathan Ho, William Chan, Chitwan Saharia, Jay Whang, Ruiqi Gao, Alexey Gritsenko, Diederik P Kingma, Ben Poole, Mohammad Norouzi, David J Fleet, et al. Imagen video: High definition video generation with diffusion models. *arXiv preprint arXiv:2210.02303*, 2022. 2
- [22] Jonathan Ho, Chitwan Saharia, William Chan, David J Fleet, Mohammad Norouzi, and Tim Salimans. Cascaded diffusion models for high fidelity image generation. *Journal of Machine Learning Research*, 23(47):1–33, 2022. 8
- [23] Vincent Tao Hu, Stefan Andreas Baumann, Ming Gui, Olga Grebenkova, Pingchuan Ma, Johannes Fischer, and Bjorn Ommer. Zigma: Zigzag mamba diffusion model. *arXiv preprint arXiv:2403.13802*, 2024. 2, 4, 6
- [24] Tero Karras, Samuli Laine, and Timo Aila. A style-based generator architecture for generative adversarial networks. In *Proceedings of the IEEE/CVF conference on computer vision and pattern recognition*, pages 4401–4410, 2019. 6
- [25] Jungo Kasai, Hao Peng, Yizhe Zhang, Dani Yogatama, Gabriel Ilharco, Nikolaos Pappas, Yi Mao, Weizhu Chen, and Noah A Smith. Finetuning pretrained transformers into rnns. *arXiv preprint arXiv:2103.13076*, 2021. 2
- [26] Angelos Katharopoulos, Apoorv Vyas, Nikolaos Pappas, and François Fleuret. Transformers are rnns: Fast autoregressive transformers with linear attention. In *International conference on machine learning*, pages 5156–5165. PMLR, 2020. 2, 3
- [27] Diederik P Kingma and Max Welling. Auto-encoding variational bayes. *arXiv preprint arXiv:1312.6114*, 2013. 7
- [28] Diederik P Kingma and Max Welling. Auto-encoding variational bayes. *arXiv preprint arXiv:1312.6114*, 2013. 5

- [29] Zhifeng Kong, Wei Ping, Jiayi Huang, Kexin Zhao, and Bryan Catanzaro. Diffwave: A versatile diffusion model for audio synthesis. *arXiv preprint arXiv:2009.09761*, 2020. 2
- [30] Tuomas Kynkäänniemi, Tero Karras, Samuli Laine, Jaakko Lehtinen, and Timo Aila. Improved precision and recall metric for assessing generative models. *Advances in neural information processing systems*, 32, 2019. 7
- [31] Yann LeCun, Léon Bottou, Yoshua Bengio, and Patrick Haffner. Gradient-based learning applied to document recognition. *Proceedings of the IEEE*, 86(11):2278–2324, 1998. 2
- [32] Cheng Lu, Yuhao Zhou, Fan Bao, Jianfei Chen, Chongxuan Li, and Jun Zhu. Dpm-solver: A fast ode solver for diffusion probabilistic model sampling in around 10 steps. *Advances in Neural Information Processing Systems*, 35:5775–5787, 2022. 2
- [33] Xin Ma, Yaohui Wang, Gengyun Jia, Xinyuan Chen, Ziwei Liu, Yuan-Fang Li, Cunjian Chen, and Yu Qiao. Latte: Latent diffusion transformer for video generation. *arXiv preprint arXiv:2401.03048*, 2024. 2
- [34] Huanru Henry Mao. Fine-tuning pre-trained transformers into decaying fast weights. *arXiv preprint arXiv:2210.04243*, 2022. 4
- [35] Kangfu Mei and Vishal Patel. Vidm: Video implicit diffusion models. In *Proceedings of the AAAI Conference on Artificial Intelligence*, pages 9117–9125, 2023. 2
- [36] Charlie Nash, Jacob Menick, Sander Dieleman, and Peter W Battaglia. Generating images with sparse representations. *arXiv preprint arXiv:2103.03841*, 2021. 6, 7
- [37] Alexander Quinn Nichol and Prafulla Dhariwal. Improved denoising diffusion probabilistic models. In *International conference on machine learning*, pages 8162–8171. PMLR, 2021. 2
- [38] William Peebles and Saining Xie. Scalable diffusion models with transformers. In *Proceedings of the IEEE/CVF International Conference on Computer Vision*, pages 4195–4205, 2023. 2, 3, 4, 5, 6, 7, 8
- [39] Bo Peng, Eric Alcaide, Quentin Anthony, Alon Albalak, Samuel Arcadinho, Huanqi Cao, Xin Cheng, Michael Chung, Matteo Grella, Kranthi Kiran GV, et al. Rwkv: Reinventing rnns for the transformer era. *arXiv preprint arXiv:2305.13048*, 2023. 2
- [40] Ethan Perez, Florian Strub, Harm De Vries, Vincent Dumoulin, and Aaron Courville. Film: Visual reasoning with a general conditioning layer. In *Proceedings of the AAAI conference on artificial intelligence*, 2018. 6
- [41] Hao Phung, Quan Dao, Trung Tuan Dao, Hoang Phan, Dimitris N Metaxas, and Anh Tuan Tran. Dimsum: Diffusion mamba-a scalable and unified spatial-frequency method for image generation. In *The Thirty-eighth Annual Conference on Neural Information Processing Systems*. 8
- [42] Ben Poole, Ajay Jain, Jonathan T Barron, and Ben Mildenhall. Dreamfusion: Text-to-3d using 2d diffusion. *arXiv preprint arXiv:2209.14988*, 2022. 2
- [43] Zhen Qin, Dong Li, Weigao Sun, Weixuan Sun, Xuyang Shen, Xiaodong Han, Yunshen Wei, Baohong Lv, Fei Yuan, Xiao Luo, et al. Scaling transormer to 175 billion parameters. *arXiv preprint arXiv:2307.14995*, 2023. 4
- [44] Zhen Qin, Songlin Yang, and Yiran Zhong. Hierarchically gated recurrent neural network for sequence modeling. *Advances in Neural Information Processing Systems*, 36, 2024. 2
- [45] Prajit Ramachandran, Barret Zoph, and Quoc V. Le. Searching for activation functions, 2017. 4
- [46] Aditya Ramesh, Prafulla Dhariwal, Alex Nichol, Casey Chu, and Mark Chen. Hierarchical text-conditional image generation with clip latents. *arXiv preprint arXiv:2204.06125*, 1 (2):3, 2022. 2
- [47] Robin Rombach, Andreas Blattmann, Dominik Lorenz, Patrick Esser, and Björn Ommer. High-resolution image synthesis with latent diffusion models. In *Proceedings of the IEEE/CVF conference on computer vision and pattern recognition*, pages 10684–10695, 2022. 4, 5
- [48] Robin Rombach, Andreas Blattmann, Dominik Lorenz, Patrick Esser, and Björn Ommer. High-resolution image synthesis with latent diffusion models. In *Proceedings of the IEEE/CVF conference on computer vision and pattern recognition*, pages 10684–10695, 2022. 2, 7, 8
- [49] Olaf Ronneberger, Philipp Fischer, and Thomas Brox. U-net: Convolutional networks for biomedical image segmentation. In *Medical image computing and computer-assisted intervention—MICCAI 2015: 18th international conference, Munich, Germany, October 5-9, 2015, proceedings, part III 18*, pages 234–241. Springer, 2015. 2
- [50] Chitwan Saharia, William Chan, Saurabh Saxena, Lala Li, Jay Whang, Emily L Denton, Kamyar Ghasemipour, Raphael Gontijo Lopes, Burcu Karagol Ayan, Tim Salimans, et al. Photorealistic text-to-image diffusion models with deep language understanding. *Advances in neural information processing systems*, 35:36479–36494, 2022. 2
- [51] Tim Salimans, Ian Goodfellow, Wojciech Zaremba, Vicki Cheung, Alec Radford, and Xi Chen. Improved techniques for training gans. *Advances in neural information processing systems*, 29, 2016. 7
- [52] Jascha Sohl-Dickstein, Eric Weiss, Niru Maheswaranathan, and Surya Ganguli. Deep unsupervised learning using nonequilibrium thermodynamics. In *International conference on machine learning*, pages 2256–2265. PMLR, 2015. 2, 4
- [53] Jiaming Song, Chenlin Meng, and Stefano Ermon. Denoising diffusion implicit models. *arXiv preprint arXiv:2010.02502*, 2020. 2
- [54] Yang Song and Stefano Ermon. Generative modeling by estimating gradients of the data distribution. *Advances in neural information processing systems*, 32, 2019. 2
- [55] Yang Song, Jascha Sohl-Dickstein, Diederik P Kingma, Abhishek Kumar, Stefano Ermon, and Ben Poole. Score-based generative modeling through stochastic differential equations. *arXiv preprint arXiv:2011.13456*, 2020. 2
- [56] Yutao Sun, Li Dong, Shaohan Huang, Shuming Ma, Yuqing Xia, Jilong Xue, Jianyong Wang, and Furu Wei. Retentive network: A successor to transformer for large language models. *arXiv preprint arXiv:2307.08621*, 2023. 4
- [57] Yao Teng, Yue Wu, Han Shi, Xuefei Ning, Guohao Dai, Yu Wang, Zhenguo Li, and Xihui Liu. Dim: Diffusion mamba

- for efficient high-resolution image synthesis. *arXiv preprint arXiv:2405.14224*, 2024. 8
- [58] Ashish Vaswani, Noam Shazeer, Niki Parmar, Jakob Uszkoreit, Llion Jones, Aidan N Gomez, Łukasz Kaiser, and Illia Polosukhin. Attention is all you need. *Advances in neural information processing systems*, 30, 2017. 2, 3
- [59] Ashish Vaswani, Noam Shazeer, Niki Parmar, Jakob Uszkoreit, Llion Jones, Aidan N Gomez, Łukasz Kaiser, and Illia Polosukhin. Attention is all you need. *Advances in neural information processing systems*, 30, 2017. 3
- [60] Enze Xie, Junsong Chen, Junyu Chen, Han Cai, Yujun Lin, Zhekai Zhang, Muyang Li, Yao Lu, and Song Han. Sana: Efficient high-resolution image synthesis with linear diffusion transformers. *arXiv preprint arXiv:2410.10629*, 2024. 2
- [61] Jing Nathan Yan, Jiatao Gu, and Alexander M Rush. Diffusion models without attention. *arXiv preprint arXiv:2311.18257*, 2023. 4
- [62] Songlin Yang, Bailin Wang, Yikang Shen, Rameswar Panda, and Yoon Kim. Gated linear attention transformers with hardware-efficient training. *arXiv preprint arXiv:2312.06635*, 2023. 2, 4, 6
- [63] Xiulong Yang, Sheng-Min Shih, Yinlin Fu, Xiaoting Zhao, and Shihao Ji. Your vit is secretly a hybrid discriminative-generative diffusion model. *arXiv preprint arXiv:2208.07791*, 2022. 2
- [64] Min Zhao, Fan Bao, Chongxuan Li, and Jun Zhu. Egsde: Unpaired image-to-image translation via energy-guided stochastic differential equations. *Advances in Neural Information Processing Systems*, 35:3609–3623, 2022. 2
- [65] Zhizhuo Zhou and Shubham Tulsiani. Sparsefusion: Distilling view-conditioned diffusion for 3d reconstruction. In *Proceedings of the IEEE/CVF Conference on Computer Vision and Pattern Recognition*, pages 12588–12597, 2023. 2

DiG: Scalable and Efficient Diffusion Models with Gated Linear Attention

Supplementary Material

ImageNet 512×512

Model	FID↓	sFID↓	IS↑	P↑	R↑
DiT-XL/2 (400K)	20.94	6.78	66.30	0.74	0.58
DiG-XL/2 (400K)	17.36	6.12	69.42	0.75	0.63

Table 6. Comparing the proposed DiG against DiT on Imagenet 512×512 benchmark.

6. Comparison on Larger Image Size

We additionally compare the performance of our plain DiG-XL/2 and DiT-XL/2 on ImageNet 512×512 class-conditional image generation. As shown in Table 6, DiG-XL/2 outperforms DiT-XL/2 under the same training iterations.

7. Details of Different Scanning Strategies

As mentioned in Section 3.3, traditional multi-path scanning methods of causal modeling often lead to numerical instability and complex extra operations. Algorithm 2, Algorithm 3, and Algorithm 4 present the details of different scanning methods, respectively. “GLA” is the scanning operator. “flip”, “reshape2d”, “transpose”, “flatten”, and “+” are the matrix operators. It can be seen that bidirectional scanning and 4-directional scanning require many extra matrix operations and scanning operations.

Algorithm 2: Bidirectional Scanning.

Input: token sequence $\mathbf{z}_{in} : (\mathbf{B}, \mathbf{T}, \mathbf{D})$
Output: token sequence $\mathbf{z}_{out} : (\mathbf{B}, \mathbf{T}, \mathbf{D})$

- 1 $\mathbf{z}'_{out,1} : (\mathbf{B}, \mathbf{T}, \mathbf{D}) \leftarrow \mathbf{GLA}(\mathbf{z}_{in})$
 /* Extra Operations */
- 2 $\mathbf{z}_{in,2} : (\mathbf{B}, \mathbf{T}, \mathbf{D}) \leftarrow \mathbf{flip}(\mathbf{z}_{in})$
- 3 $\mathbf{z}'_{out,2} : (\mathbf{B}, \mathbf{T}, \mathbf{D}) \leftarrow \mathbf{GLA}(\mathbf{z}_{in,2})$
 /* Flip the sequence to ensure the same direction as $\mathbf{z}_{out,1}$ */
- 4 $\mathbf{z}'_{out,2 \rightarrow 1} : (\mathbf{B}, \mathbf{T}, \mathbf{D}) \leftarrow \mathbf{flip}(\mathbf{z}'_{out,2})$
- 5 $\mathbf{z}_{out} : (\mathbf{B}, \mathbf{T}, \mathbf{D}) \leftarrow \mathbf{z}'_{out,1} + \mathbf{z}'_{out,2 \rightarrow 1}$
- 6 Return: \mathbf{z}_{out}

8. Additional Visualizations

We also present additional visualizations of DiG-XL/2 with resolutions of 256×256 and 512×512 in Figure 8- 19.

Algorithm 3: 4-directional Scanning.

Input: token sequence $\mathbf{z}_{in} : (\mathbf{B}, \mathbf{T}, \mathbf{D})$
Output: token sequence $\mathbf{z}_{out} : (\mathbf{B}, \mathbf{T}, \mathbf{D})$

- 1 $\mathbf{z}'_{out,1} : (\mathbf{B}, \mathbf{T}, \mathbf{D}) \leftarrow \mathbf{GLA}(\mathbf{z}_{in})$
 /* Extra Operations */
- 2 $\mathbf{z}_{in,2} : (\mathbf{B}, \mathbf{T}, \mathbf{D}) \leftarrow \mathbf{flip}(\mathbf{z}_{in})$
- 3 $\mathbf{z}'_{out,2} : (\mathbf{B}, \mathbf{T}, \mathbf{D}) \leftarrow \mathbf{GLA}(\mathbf{z}_{in,2})$
 /* Flip the sequence to ensure the same direction as $\mathbf{z}_{out,1}$ */
- 4 $\mathbf{z}'_{out,2 \rightarrow 1} : (\mathbf{B}, \mathbf{T}, \mathbf{D}) \leftarrow \mathbf{flip}(\mathbf{z}'_{out,2})$
- 5 $\mathbf{z}_{in,3} : (\mathbf{B}, \mathbf{T}, \mathbf{D}) \leftarrow$
 $\mathbf{flatten}(\mathbf{transpose}(\mathbf{reshape2d}(\mathbf{z}_{in})))$
- 6 $\mathbf{z}'_{out,3} : (\mathbf{B}, \mathbf{T}, \mathbf{D}) \leftarrow \mathbf{GLA}(\mathbf{z}_{in,3})$
- 7 $\mathbf{z}'_{out,3 \rightarrow 1} : (\mathbf{B}, \mathbf{T}, \mathbf{D}) \leftarrow$
 $\mathbf{flatten}(\mathbf{transpose}(\mathbf{reshape2d}(\mathbf{z}'_{out,3})))$
- 8 $\mathbf{z}_{in,4} : (\mathbf{B}, \mathbf{T}, \mathbf{D}) \leftarrow \mathbf{flip}(\mathbf{z}_{in,3})$
- 9 $\mathbf{z}'_{out,4} : (\mathbf{B}, \mathbf{T}, \mathbf{D}) \leftarrow \mathbf{GLA}(\mathbf{z}_{in,4})$
- 10 $\mathbf{z}'_{out,4 \rightarrow 1} : (\mathbf{B}, \mathbf{T}, \mathbf{D}) \leftarrow$
 $\mathbf{flatten}(\mathbf{transpose}(\mathbf{reshape2d}(\mathbf{flip}(\mathbf{z}'_{out,4}))))$
- 11 $\mathbf{z}_{out} : (\mathbf{B}, \mathbf{T}, \mathbf{D}) \leftarrow$
 $\mathbf{z}'_{out,1} + \mathbf{z}'_{out,2 \rightarrow 1} + \mathbf{z}'_{out,3 \rightarrow 1} + \mathbf{z}'_{out,4 \rightarrow 1}$
- 12 Return: \mathbf{z}_{out}

Algorithm 4: Block-by-Block Scanning.

Input: token sequence $\mathbf{z}_{in} : (\mathbf{B}, \mathbf{T}, \mathbf{D})$
Output: token sequence $\mathbf{z}_{out} : (\mathbf{B}, \mathbf{T}, \mathbf{D})$

- 1 $\mathbf{z}'_{out} : (\mathbf{B}, \mathbf{T}, \mathbf{D}) \leftarrow \mathbf{GLA}(\mathbf{z}_{in})$
 /* Extra Operations */
- 2 **if** $l \% 2 == 0$ **then**
- 3 $\mathbf{z}_{out} : (\mathbf{B}, \mathbf{T}, \mathbf{D}) \leftarrow \mathbf{flip}(\mathbf{z}'_{out})$
- 4 **end**
- 5 **else**
- 6 $\mathbf{z}_{out} : (\mathbf{B}, \mathbf{T}, \mathbf{D}) \leftarrow$
 $\mathbf{flatten}(\mathbf{transpose}(\mathbf{reshape2d}(\mathbf{z}'_{out})))$
- 7 **end**
- 8 Return: \mathbf{z}_{out}



Figure 8. **Uncurated** 256×256 DiG-XL/2 samples.
Classifier-free guidance scale = 4.0
Class label = "golden retriever" (207)



Figure 9. **Uncurated** 256×256 DiG-XL/2 samples.
Classifier-free guidance scale = 4.0
Class label = "husky" (250)



Figure 10. **Uncurated** 256×256 DiG-XL/2 samples.
 Classifier-free guidance scale = 4.0
 Class label = "arctic fox" (279)



Figure 11. **Uncurated** 256×256 DiG-XL/2 samples.
 Classifier-free guidance scale = 4.0
 Class label = "volcano" (980)



Figure 12. **Uncurated** 256×256 DiG-XL/2 samples.
 Classifier-free guidance scale = 4.0
 Class label = "loggerhead sea turtle" (33)



Figure 13. **Uncurated** 256×256 DiG-XL/2 samples.
 Classifier-free guidance scale = 4.0
 Class label = "sulphur-crested cockatoo" (89)



Figure 14. **Uncurated** 512×512 DiG-XL/2 samples.
 Classifier-free guidance scale = 4.0
 Class label = "macaw" (88)



Figure 15. **Uncurated** 512×512 DiG-XL/2 samples.
 Classifier-free guidance scale = 4.0
 Class label = "arctic wolf" (270)

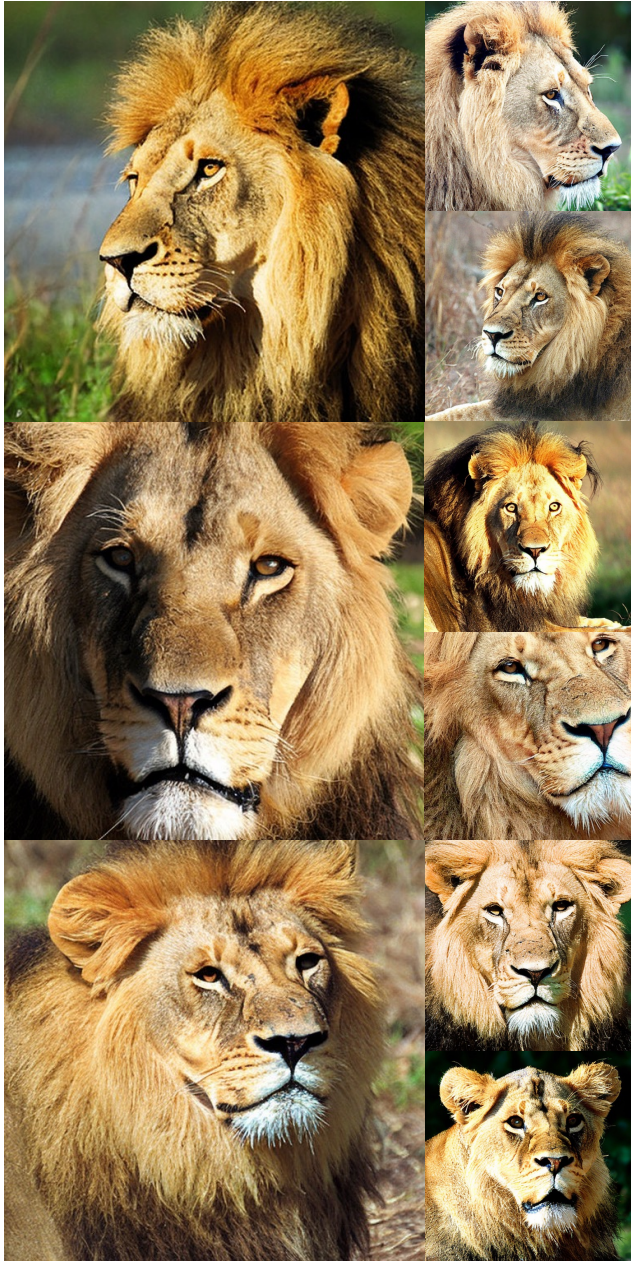


Figure 16. **Uncurated** 512×512 DiG-XL/2 samples.
Classifier-free guidance scale = 4.0
Class label = "lion" (291)



Figure 17. **Uncurated** 512×512 DiG-XL/2 samples.
Classifier-free guidance scale = 4.0
Class label = "red panda" (387)



Figure 18. **Uncurated** 512×512 DiG-XL/2 samples.
 Classifier-free guidance scale = 4.0
 Class label = "panda" (388)



Figure 19. **Uncurated** 512×512 DiG-XL/2 samples.
 Classifier-free guidance scale = 4.0
 Class label = "ice cream" (928)